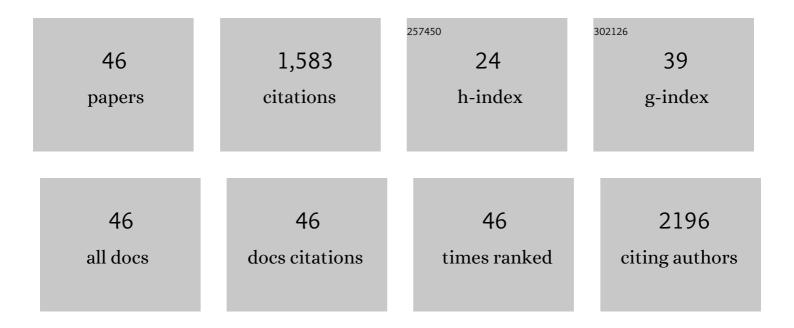
Andreas

List of Publications by Year in descending order

Source: https://exaly.com/author-pdf/7619626/publications.pdf Version: 2024-02-01



#	Article	IF	CITATIONS
1	New method for quantification of intratumoral heterogeneity: a feasibility study on Ktrans maps from preclinical DCE-MRI. Magnetic Resonance Materials in Physics, Biology, and Medicine, 2021, 34, 845-857.	2.0	2
2	NRL and CRX Define Photoreceptor Identity and Reveal Subgroup-Specific Dependencies in Medulloblastoma. Cancer Cell, 2018, 33, 435-449.e6.	16.8	52
3	<i>T</i> ₂ *â€relaxivity contrast imaging: First results. Magnetic Resonance in Medicine, 2013, 69, 1430-1437.	3.0	12
4	Meningioma progression in mice triggered by Nf2 and Cdkn2ab inactivation. Oncogene, 2013, 32, 4264-4272.	5.9	41
5	Radial multigradient-echo DCE-MRI for 3D <i>K</i> ^{trans} mapping with individual arterial input function measurement in mouse tumor models. Magnetic Resonance in Medicine, 2013, 70, 823-828.	3.0	4
6	Age-related cerebral atrophy in nonhuman primates predicts cognitive impairments. Neurobiology of Aging, 2012, 33, 1096-1109.	3.1	69
7	Increased regional cerebral glucose uptake in an APP/PS1 model of Alzheimer's disease. Neurobiology of Aging, 2012, 33, 1995-2005.	3.1	95
8	Age-associated cerebral atrophy in mouse lemur primates. Neurobiology of Aging, 2011, 32, 894-906.	3.1	72
9	Detection of vascular alterations by in vivo magnetic resonance angiography and histology in APP/PS1 mouse model of Alzheimer's disease. Magnetic Resonance Materials in Physics, Biology, and Medicine, 2010, 23, 53-64.	2.0	24
10	2D and 3D radial multiâ€gradientâ€echo DCE MRI in murine tumor models with dynamic <i>R</i> * ₂ â€corrected <i>R</i> ₁ mapping. Magnetic Resonance in Medicine, 2010, 64, 313-318.	3.0	11
11	Tumor tissue analysis by self organizing maps from combined DCE-/DSC-MRI data. , 2009, , .		1
12	<i>In vitro</i> setup to study permeability characteristics of contrast agents by MRI. Contrast Media and Molecular Imaging, 2009, 4, 66-72.	0.8	11
13	Bolusâ€ŧracking MRI with a simultaneous <i>T</i> ₁ ―and <i>T</i> â€measurement. Magnetic Resonance in Medicine, 2009, 62, 672-681.	3.0	38
14	Characterization of in vivo MRI detectable thalamic amyloid plaques from APP/PS1 mice. Neurobiology of Aging, 2009, 30, 41-53.	3.1	53
15	23Na MRI longitudinal follow-up of PDT in a xenograft model of human retinoblastoma. Photodiagnosis and Photodynamic Therapy, 2009, 6, 214-220.	2.6	42
16	Magnetic resonance imaging and histological studies of corpus callosal and hippocampal abnormalities linked to <i>doublecortin</i> deficiency. Journal of Comparative Neurology, 2007, 500, 239-254.	1.6	64
17	Transverse relaxation time reflects brain amyloidosis in young APP/PS1 transgenic mice. Magnetic Resonance in Medicine, 2007, 58, 179-184.	3.0	30
18	Simultaneous dynamic T 1 and T 2 * measurement for AIF assessment combined with DCE MRI in a mouse tumor model. Magnetic Resonance Materials in Physics, Biology, and Medicine, 2007, 20, 193-203.	2.0	35

ANDREAS

#	Article	IF	CITATIONS
19	Early Effects of Combretastatin A4 Phosphate Assessed by Anatomic and Carbogen-Based Functional Magnetic Resonance Imaging on Rat Bladder Tumors Implanted in Nude Mice. Neoplasia, 2006, 8, 587-595.	5.3	10
20	In vivo MRI and histological evaluation of brain atrophy in APP/PS1 transgenic mice. Neurobiology of Aging, 2006, 27, 835-847.	3.1	91
21	Age-related evolution of amyloid burden, iron load, and MR relaxation times in a transgenic mouse model of Alzheimer's disease. Neurobiology of Disease, 2006, 22, 199-208.	4.4	79
22	Passive staining: A novel ex vivo MRI protocol to detect amyloid deposits in mouse models of Alzheimer's disease. Magnetic Resonance in Medicine, 2006, 55, 687-693.	3.0	37
23	An efficient design for birdcage probes dedicated to small-animal imaging experiments. Magnetic Resonance Materials in Physics, Biology, and Medicine, 2004, 17, 363-371.	2.0	6
24	Relationship between tumour growth rate and carbogen-based functional MRI for a chemically induced HCC in mice. Magnetic Resonance Materials in Physics, Biology, and Medicine, 2004, 17, 271-280.	2.0	11
25	Morphological and carbogen-based functional MRI of a chemically induced liver tumor model in mice. Magnetic Resonance in Medicine, 2003, 50, 522-530.	3.0	24
26	Regional atrophy in the brain of lissencephalic mouse lemur primates: Measurement by automatic histogram-based segmentation of MR images. Magnetic Resonance in Medicine, 2003, 50, 984-992.	3.0	30
27	On the use ofR1 andR2* for measurement of contrast agent concentration in isolated perfused rat liver. NMR in Biomedicine, 2003, 16, 276-285.	2.8	4
28	In vivo gallbladder bile diffusion coefficient measurement by diffusion-weighted echo planar imaging in hamster fed normal and lithogenic diets. Magnetic Resonance in Medicine, 2000, 43, 854-859.	3.0	2
29	High-resolution proton nuclear magnetic resonance spectroscopy of ovarian cyst fluid. NMR in Biomedicine, 2000, 13, 297-305.	2.8	87
30	Directin vivo observation of 5-fluorouracil release from a prodrug in human tumors heterotransplanted in nude mice: a magnetic resonance study. NMR in Biomedicine, 2000, 13, 306-310.	2.8	25
31	MRI description of cerebral atrophy in mouse lemur primates. Neurobiology of Aging, 2000, 21, 81-88.	3.1	48
32	Stroke outcome determination with a prefabricated fibrin-rich macroclot in a thromboembolic rat middle cerebral artery occlusion model. Fibrinolysis and Proteolysis, 1999, 13, 193-201.	1.1	0
33	Cerebral T2-Weighted Signal Decrease During Aging in the Mouse Lemur Primate Reflects Iron Accumulation. Neurobiology of Aging, 1998, 19, 65-69.	3.1	87
34	T2-weighted MRI Studies of Mouse Lemurs: A Primate Model of Brain Aging. Neurobiology of Aging, 1997, 18, 517-521.	3.1	26
35	Age dependence of the T2-weighted MRI signal in brain structures of a prosimian primate (Microcebus) Tj ETQq	1 1 0.7843 2.1	14 _g gBT /Ove
36	The effects of a butanediol treatment on acute focal cerebral ischemia assessed by quantitative	1.8	3

diffusion and T2 MR imaging. Magnetic Resonance Imaging, 1997, 15, 1045-1055.

1.8 3

ANDREAS

#	Article	IF	CITATIONS
37	Spreading of Vasogenic Edema and Cytotoxic Edema Assessed by Quantitative Diffusion and T2 Magnetic Resonance Imaging. Stroke, 1997, 28, 419-427.	2.0	181
38	A New Model of Experimental Prosthetic Joint Infection Due to Methicillin-Resistant Staphylococcus aureus: A Microbiologic, Histopathologic, and Magnetic Resonance Imaging Characterization. Journal of Infectious Diseases, 1996, 174, 414-417.	4.0	81
39	Magnetic resonance imaging for the visualization of cholesterol gallstones in hamster fed a new high sucrose lithogenic diet. Journal of Hepatology, 1995, 22, 486-494.	3.7	15
40	Comparative NMR study of a differentiated rat hepatoma and its dedifferentiated subclone cultured as spheroids and as implanted tumors. NMR in Biomedicine, 1994, 7, 278-286.	2.8	19
41	An experimental approach for dynamic rat liver observationin vivo andex vivo by31P localized MR spectroscopy for follow-up of liver status at different steps of orthotopic transplantation–a feasibility study. NMR in Biomedicine, 1994, 7, 366-373.	2.8	3
42	Evaluation of a rabbit model for osteomyelitis by high field, high resolution imaging using the chemical-shift-specific-slice-selection technique. Magnetic Resonance Imaging, 1994, 12, 1039-1046.	1.8	17
43	Heteronuclear directed site-selective NOESY spectroscopy by polarization transfer or multiple quantum filtering. Magnetic Resonance in Chemistry, 1988, 26, 78-84.	1.9	2
44	High-resolution localized spectroscopy at 4.7 tesla by frequency-interval-Selective volume localization (FRIVOL). Journal of Magnetic Resonance, 1988, 76, 386-392.	0.5	1
45	Chemical shift-specific slice selection. A new method for chemical shift imaging at high magnetic field. Journal of Magnetic Resonance, 1987, 71, 168-174.	0.5	22
46	Two-dimensional heteronuclear relayed incoherent transfer spectroscopy. Journal of Magnetic Resonance, 1985, 63, 605-611.	0.5	8